Available online at www.sciencedirect.com

SciVerse ScienceDirect

Ceramics International 39 (2013) 3893–3899

CERAMICS INTERNATIONAL

www.elsevier.com/locate/ceramint

A thermodynamically stable $La_2NiO_{4+\delta}$/ $Gd_{0.1}Ce_{0.9}O_{1.95}$ bilayer oxygen transport membrane in membrane-assisted water splitting for hydrogen production

Sang-Yun Jeon[a], Ha-Ni Im[a], Bhupendra Singh[a], Jin-Ha Hwang[b], Sun-Ju Song[a,*]

[a]Department of Materials Science and Engineering, Chonnam National University,77 Yongbong-ro, Buk-gu, Gwangju, 500-757, Korea
[b]Department of Materials Science and Engineering, Hongik University, 94 Wausan-ro, Mapo-gu, Seoul, 121-791, Korea

Received 20 September 2012; received in revised form 22 October 2012; accepted 22 October 2012
Available online 26 October 2012

Abstract

A bilayer configuration of mixed ion-electron conducting $La_2NiO_{4+\delta}$ and oxygen-ion conducting $Gd_{0.1}Ce_{0.9}O_{1.95}$ (LNO/GDC10) was proposed for hydrogen production by water-splitting and its properties were measured as a function of temperature, reducing gas CO content and water vapor pressure during the hydrogen production by water-splitting. The hydrogen production flux increased with increasing water vapor pressure and oxygen chemical potential to a maximum of 0.12 cm^3 (STP)/min-cm^2 with 23.25% CO/76.75% CO_2 (40 sccm)/balance He (60 sccm) gas mixture on the oxygen-permeate side and wet N_2 ($pH_2O=0.49$ atm) on the oxidizing side at 900 °C. The stability of the bilayer membrane was tested in a very low oxygen partial pressure (pO_2) on the oxygen-permeate side. The presence of GDC10 on the oxygen-permeate side of the bilayer prevented the direct exposure of LNO to very low pO_2 and thus protected it from decomposition, even at $pO_2 \approx 10^{-15}$ atm.

Keywords: $La_2NiO_{4+\delta}$/ $Gd_{0.1}Ce_{0.9}O_{1.95}$ bilayer; Water-splitting; Hydrogen production; Membrane-assisted water splitting for hydrogen production

1. Introduction

Inorganic membranes have been extensively studied for hydrogen production and purification due to the ever increasing demand for high purity hydrogen in fuel cells, and petrochemical and semiconductor applications [1–5]. Among these inorganic membranes, mixed ion-electron conducting (MIEC) dense ceramic membranes have attracted major attention for gas separation applications [1,3,5–7] because of their ability to separate oxygen from a gaseous mixture by non-galvanic ambipolar transport of oxygen from the high oxygen partial pressure side (pO_2) to the low pO_2 side, when placed in a chemical potential gradient of oxygen. Moreover, when MIEC membranes are coupled with the water dissociation process, they can be utilized for hydrogen production at even moderate temperatures by selectively removing oxygen from the reaction system in Eq. (1)

$$H_2O \leftrightarrow H_2 + \frac{1}{2}O_2 \quad (1)$$

by non-galvanic ambipolar transport of oxygen and, thereby, shifting the thermodynamic equilibrium of the reaction to the product side [1,6,7]. Since the membrane-assisted water-splitting for hydrogen production (MWHP) is a direct result of oxygen permeation through membranes, the oxygen permeation rate is an important factor in determining the hydrogen production rate.

The factors affecting the oxygen permeation rate and, in turn, the hydrogen production rate by water-splitting include (i) ambipolar (oxygen ion and electron) conductivity, (ii) pO_2 gradient across the membrane, (iii) temperature, (iv) membrane thickness, and (v) surface oxygen exchange kinetics [7,8]. For MWHP using MIEC membranes at moderate temperatures, the creation of a high pO_2 gradient across the membrane is an important factor. However, as the equilibrium constant of reaction in Eq. (1)

*Corresponding author. Tel.: +1 82 62 530 1706; fax: +1 82 62 530 1699.
E-mail addresses: song@jnu.ac.kr, song@chonnam.ac.kr (S.-J. Song).

0272-8842/$ - see front matter © 2012 Elsevier Ltd and Techna Group S.r.l. All rights reserved.
http://dx.doi.org/10.1016/j.ceramint.2012.10.233

is very small [9], the actual concentration of oxygen formed by water-splitting and the resultant pO_2 on the oxidizing side are very small in magnitude. Therefore, to create a high pO_2 gradient across the membrane, the pO_2 on the reducing side of the membrane should be lower in the magnitude than the pO_2 of the oxidizing side. In the past, most MWHP research has focused on proving the working principle of hydrogen production using MIEC membranes without paying greater attention to the thermodynamic stability of these membranes during the operation [1,6,10]. However, the requirement for very low pO_2 on the reducing side of the oxygen permeation membrane creates a major challenge for the application of MIECs in MWHP, as MIECs are prone to decomposition at very low pO_2, which raises serious concerns about the thermodynamic stability of such membranes in working environments [11,12]. In this study, we have addressed the problem of the thermodynamic stability of MIEC membranes during MWHP by utilizing the concept of bilayered membrane using lanthanum nickel oxide ($La_2NiO_{4+\delta}$, LNO) as an MIEC material.

LNO with K_2NiF_4-type structure exhibits one of the highest oxygen permeation fluxes among alkaline-earth metal cation-free membrane materials [13]. Apart from their high oxygen permeability, LNO-based materials offer additional advantages of moderate thermal expansion that is compatible with glass-ceramic sealants and stainless steel, very low chemically induced stress and reduced interaction with gaseous species such as CO_2 due to the absence of alkaline-earth cations. Therefore, as we have previously reported [14], the LNO-based MIEC materials have potential for application in oxygen separation membranes. However, like other MIEC materials, LNO suffers from instability in low pO_2 environment [15,16]. Therefore, in order to overcome the limited thermodynamic stability of LNO in a low pO_2 atmosphere during MWHP, in the present work, we demonstrate the concept of a bilayer membrane consisting of LNO and 10% gadolinium-doped ceria ($Gd_{0.1}Ce_{0.9}O_{1.95}$, GDC10). In a bilayer structure, as shown in Fig. 1(a), the gradient within each layer is determined by the relative thickness and transport property of the individual layer [11], so that the local oxygen activity at the material interface between LNO and GDC10 can be increased by increasing the thickness of the GDC10 layer relative to the LNO layer. In this way, the pO_2 at the GDC10/LNO interface can be increased to a point where the LNO alone would be thermodynamically unstable in a reducing atmosphere. Therefore, by using a 'protective layer' of GDC10 on the reducing gas side, the stability of the otherwise thermodynamically unstable LNO-based material in a reducing atmosphere is ensured, as it is not exposed directly to a lower pO_2 and the consequent LNO decomposition. LNO is used as the MIEC in the present study due to its high oxygen permeation rate as compared to the other MIECs that are relatively more stable in low pO_2, such as $La_{0.7}Sr_{0.3}Cu_{0.2}Fe_{0.8}O_{3-\delta}$ (LSCF7328) [1]. Although LNO decomposes at higher pO_2 than LSCF7328, its oxygen

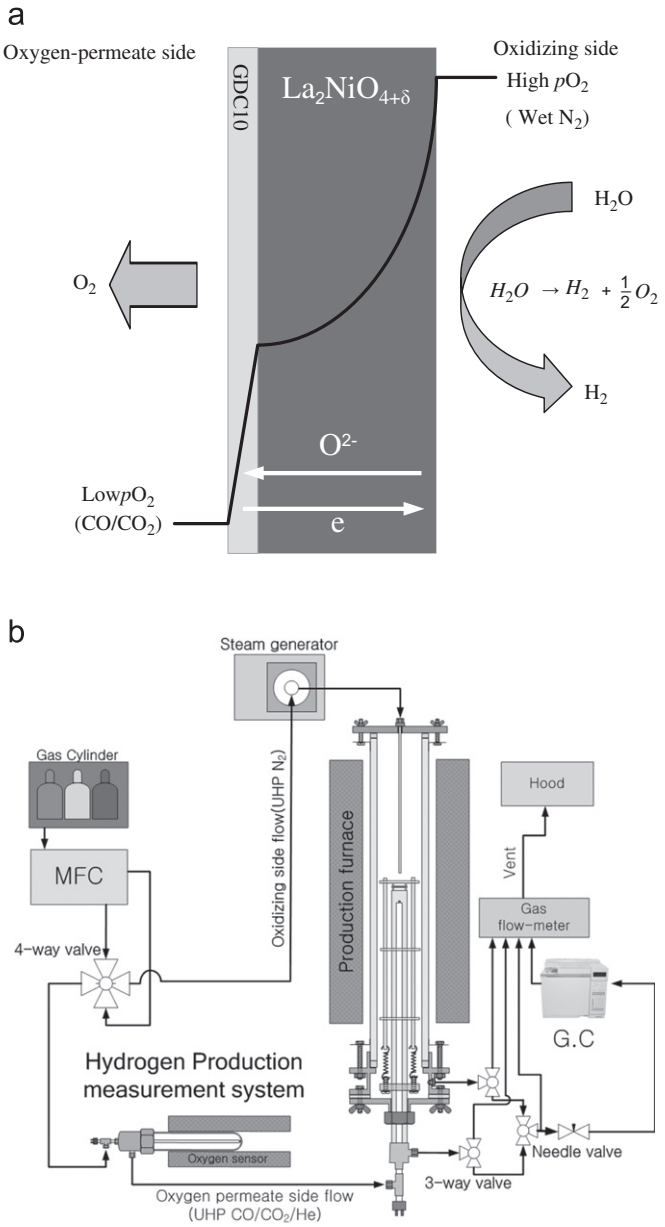

Fig. 1. Schematic diagram of (a) the operation of LNO/GDC10 bilayer membrane in hydrogen production using water splitting and (b) the experimental set-up of hydrogen production from water splitting using LNO/GDC10 bilayer membrane.

permeation rate is higher than that of LSCF7328, when compared under a thickness-normalized condition (≈ 0.954 mm) at different temperatures [14]. Ceria-based solid oxides show a higher stability in a very low pO_2 atmosphere [17] and are normally used as oxide ion-conducting electrolytes. However, they easily develop n-type electronic conduction at high temperatures and low pO_2 [18]. Therefore, the use of GDC10 in bilayer fabrication not only improves the compatibility between the LNO and GDC10 layers under reducing conditions but also ensures good ambipolar diffusion of oxygen in the bilayer membrane. In this work, a LNO/GDC10 bilayer is fabricated by slurry coating method and then investigated

as an oxygen permeation membrane for MWHP with a gas mixture (CO/CO_2)/balance He as a reducing gas on the oxygen-permeate side and wet N_2 gas on the oxidizing side of the membrane at different temperatures and under a range of pO_2 low enough to decompose LNO. The hydrogen production rate is examined as a function of temperature, water vapor pressure (pH_2O) and CO content.

2. Materials and methods

2.1. Fabrication of LNO/GDC10 bilayer membrane

Undoped LNO powder was prepared using lanthanum(III) acetate hydrate (99.9%, Aldrich, USA) and nickel(II) acetate tetrahydrate (99.9%, Aldrich, USA) as the starting materials by a coprecipitation method similar to that previously reported [19]. The calcined power was uniaxially pressed into disks of ~19 mm diameter and then sintered at 900 °C for 5 h in air. For the fabrication of a LNO/GDC10 double layer, a coating slurry of GDC10 (Kceracell, BET = 10–15 m^2/g, d50 = 0.3–0.6 μm) was separately prepared in an ethanol-based solvent [20,21] and then was spin-coated onto the LNO disk. For the GDC10 slurry preparation, GDC10 was ball milled with 1 wt% dispersant (Solsperse® 24000 SC/GR) in ethanol for 24 h, followed by the addition of a plasticizer (dibenzyl phthalate, 2 wt%) and a binder (polyvinyl butyral, 10 wt%) and subsequent ball-milling the mixture for 24 h. The LNO disks were polished with 800-grit SiC paper to give a smooth flat surface, which was then spin-coated thrice with the as-prepared GDC10 slurry to create a LNO/GDC10 bilayer disk that was finally sintered at 1300 °C for 10 h in air.

In order to evaluate the possibility of any chemical interaction between the LNO and GDC10 at the LNO/GDC10 bilayer interface during the sintering process, a disk with a 50:50 (vol%) mixture of LNO and GDC10 was prepared and sintered in the similar conditions that were used for the LNO/GDC10 bilayer disk (i.e., at 1300 °C for 10 h in air) and it was analyzed by XRD.

2.2. Characterization of LNO/GDC10 bilayer membrane

The crystalline phases in the LNO/GDC10 bilayer disk and in a LNO-GDC10 (50:50 wt %) disk were examined using an X-ray diffractometer (XRD-7000, Shimadzu) equipped with a CuK_α radiation source (1.5406 Å) and operated at 40 kV and 30 mA at a scan rate of 1°/min between scanning angles (2θ) of 20 and 80°. The microstructure of the as-sintered LNO/GDC10 bilayer disk was analyzed by scanning electron microscopy (Shimadzu, SS-550, Kyoto, Japan). A dense LNO/GDC10 bilayer disc of 15 mm diameter and 0.3 mm thickness was used for the hydrogen production process. The thickness of the LNO layer was controlled by polishing with 800-grit SiC paper before coating with GDC10.

2.3. Experimental procedure for hydrogen production from water-splitting using LNO/GDC10 bilayer membrane

Fig. 1(b) shows the schematic diagram of the experimental set-up of hydrogen production from water-splitting using LNO/GDC10 bilayer membrane. The GDC10-coated side was affixed to an alumina tube [22,23] and the GDC10 side of the bilayer was exposed to the oxygen-permeate side and the LNO side of the bilayer was exposed to the oxidizing gas side during the measurements. A wet N_2 (120 sccm) was supplied on the oxidizing gas side (i.e. the hydrogen-generation side) of the LNO/GDC bilayer. The wet N_2 stream was produced by bubbling industrial N_2 through a water-containing flask kept in a water bath (EX-35D1 heating bath, Fisher Scientific) at the controlled temperature. The pH_2O was calculated using Eq. (2) as given below.

$$P_{H_2O}/\text{atm} = P^{\infty}\exp-\{Q_{vap}/RT\} \quad (2)$$

where $P^{\infty} = (1\ \text{atm})\exp\{+Q_{vap}/RT_b\}$, ($Q_{vap}$ = 44.016 kJ/mole; T_b = 373.15 K [24]. The temperature of wet N_2 was maintained by heating the gas-supply line between the water bath and the inlet of the reactor on the oxidizing side with heating tape to avoid any condensation in the gas-supply line. The flow rate was kept constant and the wet gas stream was experimentally measured by dew-point meter DM70. A gas mixture (CO/CO_2) (40 sccm)/balance He (60 sccm) was supplied on the oxygen-permeate side (i.e., the reducing side) of the membrane to establish an oxygen potential-gradient across the membrane. The hydrogen production rate at the oxidizing gas side was analyzed with a gas chromatograph (Agilent 6890 gas chromatograph). The membrane edges were sealed with a ceramic sealant in order to minimize the edge contribution to the permeation. The gases used onto the oxidizing side and the oxygen-permeate side during the experiment were supplied at the ambient pressure [25]. The possibility of any leakage of gases through the pores in the LNO/GDC10 bilayer or due to the incomplete sealing was monitored by measuring the He content of the permeate stream and the data acquisition was performed only when the leakage rate was $< 1\%$.

3. Results and discussion

Fig. 2 shows the SEM image of the cross-section of the as-sintered LNO/GDC10 bilayer disk. The bilayer shows a well-developed and crack-free microstructure with low porosity (97% of the theoretical density). In a 0.3 mm thick LNO/GDC10 bilayer, the thickness of GDC10 layer and LNO layer was ~0.008 mm and ~0.292 mm, respectively. Both the components of the bilayer were co-sintered properly and they were well-adhered together. Fig. 3 shows the XRD pattern of the crushed disk made of the LNO-GDC10 mixture (50:50 wt%). The diffraction peaks in Fig. 3 either correspond to GDC10 or LNO and there are no additional diffraction peaks that can be assigned to any

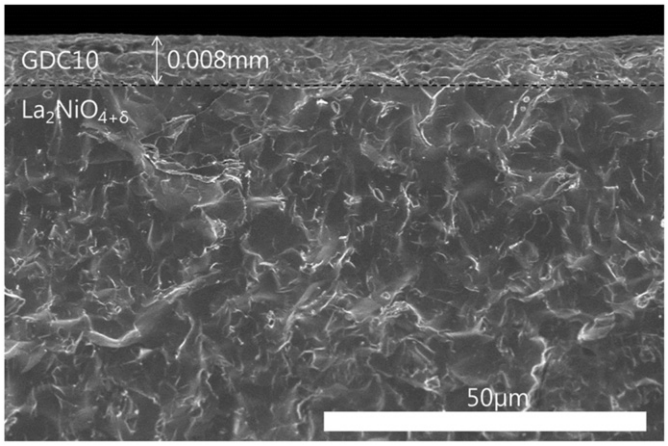

Fig. 2. SEM image of the cross-section of the LNO/GDC10 bilayer.

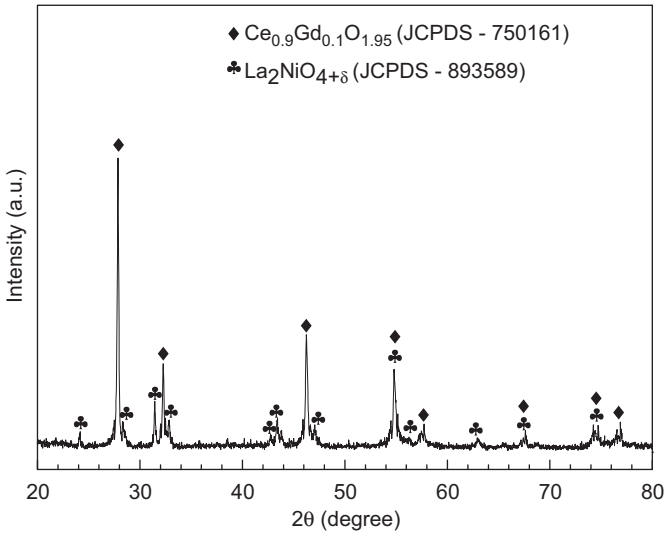

Fig. 3. XRD pattern the crushed LNO-GDC10 (50:50 vol%) disk sintered at 1300 °C for 10 h in air.

extra phase formation due to the chemical interaction between LNO and GDC10 during the co-sintering process. The above observation confirmed the absence of any chemical interaction between the two components at the interface of LNO/GDC10 bilayer during the sintering process.

The LNO/GDC10 bilayer was used in MWHP and the hydrogen production rate was measured as a function of pH_2O on the oxidizing side. Fig. 4 shows the effect of varying pH_2O on the hydrogen production rate at 900 °C using a 0.3 mm LNO/GDC10 bilayer as the oxygen diffusion membrane and wet N_2 on the oxidizing side and (4% CO/96% CO_2) (40 sccm)/balance He (60 sccm) on the oxygen-permeate side. No hydrogen was produced when the water bath temperature was 297 K ($pH_2O \approx 0.03$ atm), although the pO_2 gradient across the membrane was enough for oxygen diffusion but the pH_2O alone was not enough for water splitting. However, on raising the pH_2O to 0.07 atm ($T \approx 40$ °C) the hydrogen production rates of

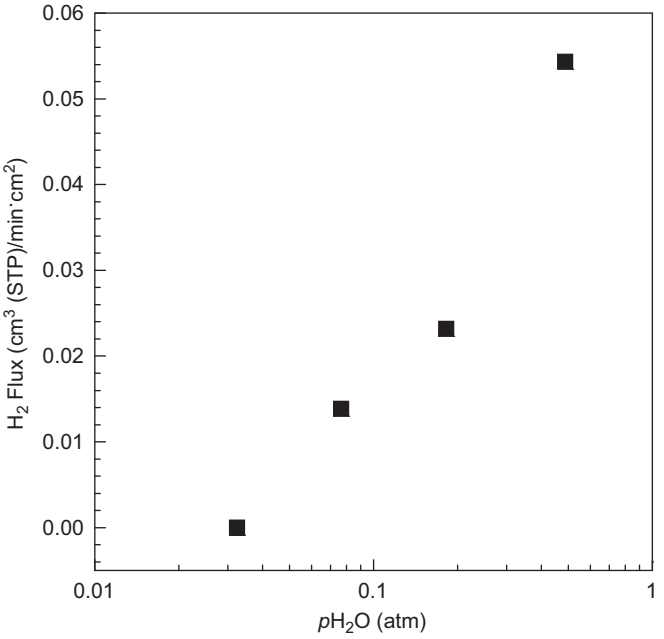

Fig. 4. Variation of hydrogen production rate on a 0.3 mm LNO/GDC10 bilayer as a function of pH_2O at 900 °C using wet N_2 on the oxidizing side and the (4% CO/96% CO_2) (40 sccm)/balance He (60 sccm) gas mixture on the oxygen-permeate side.

≈ 0.014 cm^3 (STP)/min-cm^2 was obtained, which further reached to ≈ 0.055 cm^3 (STP)/min-cm^2 on raising the pH_2O to 0.49 atm ($T \approx 81$ °C). The increased hydrogen production rate from water splitting is a direct result of oxygen removal by oxygen permeation from the oxidizing side and the results can be attributed to the increased pO_2 gradient across the LNO/GDC10 bilayer membrane for oxygen diffusion [6]. An increase in pH_2O in the oxidizing gas led to the increase in pO_2 and which, in turn, increased the driving force for O_2 permeation across the LNO/GDC10 bilayer membrane. In Fig. 4, the hydrogen production rate exhibited a logarithmic dependence on pH_2O, which was similar to the previous report of MWHP using a single layer of MIECs [6].

The hydrogen production rates were also measured with different CO content in the (CO/CO_2) (40 sccm)/balance He (60 sccm) gas mixture on the oxygen-permeate side by varying the CO content in the range of 4–23.25% relative to (CO/CO_2). The increase in CO content in the reducing gas mixture leads to decrease in pO_2 on the oxygen-permeate side and, therefore, the results of variation in CO content can be interpreted as showing the dependence of the hydrogen production rate on the pO_2 on the oxygen-permeate side. Fig. 5 shows the variation of hydrogen production rate as a function of pO_2 corresponding to CO content in the gas mixture on the oxygen-permeate side, with a 0.3 mm thick LNO/GDC10 bilayer membrane (LNO 0.292 mm and GDC10 0.008 mm) at a constant pH_2O of 0.49 atm and 900 °C. The hydrogen production rate was increased with increasing CO content because of the consequential decrease in pO_2, which, in turn, increased

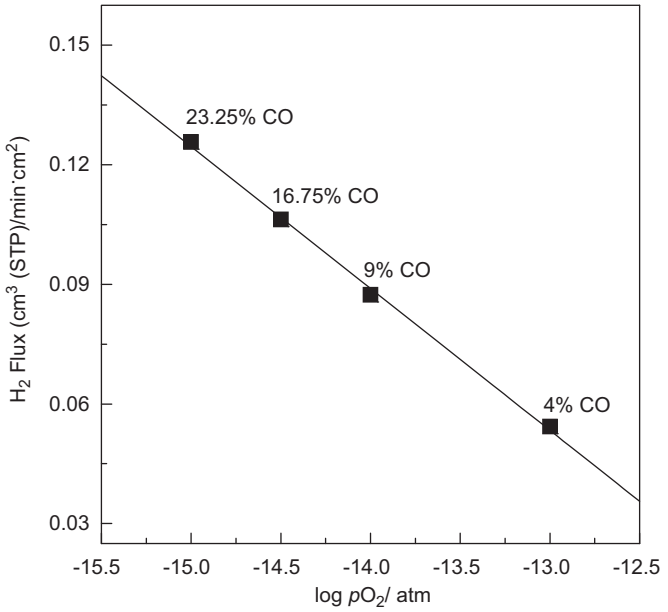

Fig. 5. Variation of hydrogen production rate on a 0.3 mm LNO/GDC10 bilayer as a function of the pO_2 on the oxygen-permeate side at 900 °C using wet N_2 ($pH_2O=0.49$ atm) on the oxidizing side and different CO content in gas mixture on the oxygen permeate side.

the driving force for the oxygen permeation from the oxidizing side to the oxygen-permeate side. Therefore, the hydrogen production flux, which was 0.0543 cm^3 (STP)/min-cm^2 at $pO_2=10^{-13}$ atm, was increased to 0.125 cm^3 (STP)/min-cm^2 at $pO_2=10^{-15}$ atm and the hydrogen production rate showed a logarithmic dependence on pO_2 on the oxygen-permeate side, as shown in Fig. 5. In the case of the MIEC membranes, the logarithmic dependence of the O_2 permeation rate on the O_2 gradient indicates that the O_2 permeation process is limited by the bulk diffusion of oxygen [26,27]. The observation of a similar logarithmic dependence of the hydrogen production rate on the pO_2 on the oxygen-permeate side using the LNO/GDC10 bilayer membrane revealed that the hydrogen production rate of the LNO/GDC10 bilayer configuration was also dominated by the bulk diffusion of oxygen under the measurement conditions.

The major objective of this study was to design a stable MWHP in very low pO_2 using an MIEC in a bilayer configuration. Therefore, in order to study the long term operational stability of the LNO/GDC10 bilayer membrane in very low pO_2, a LNO/GDC10 bilayer was used for continuous operation for 1 week at 900 °C with (23.25% CO/76.75% CO_2) (40 sccm)/balance He (60 sccm) gas mixture on the oxygen-permeate side and wet N_2 ($pH_2O=0.49$ atm) on the oxidizing side. During this duration, the hydrogen production rate showed very small variations that were within the limits of variation due to the experimental error, suggesting that the bilayer was chemically stable during water-splitting reaction with a CO-rich gas stream as the reducing gas on the oxygen-permeate side. Also, there was no increase in gas leakage during the measurements, which suggested that the LNO component of the bilayer membrane did not decompose even under very low pO_2 (log pO_2/atm = −15), although the pO_2 for the decomposition of LNO is generally equivalent to log pO_2/atm = −12.06 at 900 °C [28,29].

While using a bilayer configuration, the chemical potential gradient of each interface was different and the LNO surface at the reducing side could be protected from exposure to very low oxygen potential. Therefore, although the pO_2 on the oxygen-permeate side (i.e., the GDC10 side of the bilayer) was very low; the pO_2 at the LNO/GDC10 interface was high enough to prevent the decomposition of LNO. These results clearly confirmed that the LNO/GDC10 bilayer membrane showed good chemical resistance to carbon forming or decomposition [6,30,31] and that the bilayer configuration successfully solved the problem of instability of MIECs in low pO_2.

Fig. 6 shows the dependence of the hydrogen production rate on temperature with a 16.75% CO/83.25% CO_2 (40 sccm)/balance He (60 sccm) gas mixture on the oxygen-permeate side and wet N_2 ($pH_2O=0.49$ atm) on the oxidizing side. The variation of hydrogen production rate with temperature shows Arrhenius-type behavior, indicating a thermally activated hydrogen production process with the activation energy of 0.63 eV. Although the values of pO_2 changed with the variation of temperature, as it is given in brackets in Fig. 6, and therefore, the activation energy calculated from Fig. 6 gives only the apparent value, not the exact one, of activation energy in the pO_2 range of 10^{-15} to

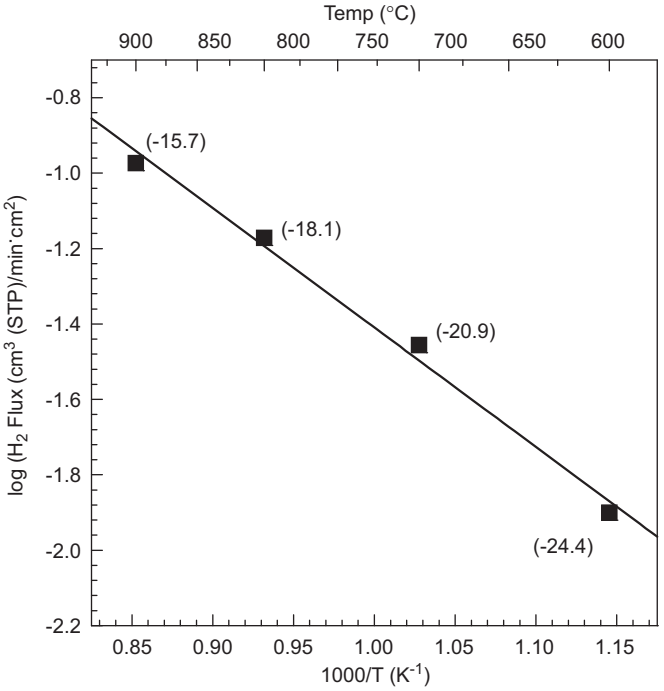

Fig. 6. The dependence of the hydrogen production rate on temperature with a 0.3 mm LNO/GDC10 bilayer using (16.75% CO/83.25%CO_2) (40 sccm)/balance He (60 sccm) gas mixture on the oxygen-permeate side and wet N_2 ($pH_2O=0.49$ atm) on the oxidizing side. Data given in brackets are log (pO_2/atm) values on the oxygen permeate-side at the corresponding temperatures.

10^{-24} atm. However, this can be useful in comparing with the other oxide ion conductors/mixed conductors. The activation energy was relatively lower than those for perovskite-mixed conductors such as LSCF7328 (≈ 0.78 eV, thickness 0.36 mm, $pO_2 \approx 10^{-14}$ atm) [31]. The normalized value of hydrogen production using LNO/GDC10 bilayer membranes was twice the value for LSCF7328 (≈ 0.04 cm^3 (STP)/min-cm^2) at 900 °C. The reported activation energy for conduction in GDC10 in the pO_2 range of 10^{-14} to 10^{-15} atm is ≈ 0.65 eV [32], which is similar to those obtained in the present study for the LNO/GDC10 bilayer. GDC, which is an oxide ion conductor in normal pO_2 conditions, develops mixed electronic-oxide ion conduction in very low pO_2 range. In order to keep GDC in the MIEC regime, pO_2 should be $< 10^{-15}$ atm at 700 °C and $< 10^{-10}$ atm at 900 °C [33]. It is clear from the pO_2 values in Fig. 6 that using bilayer configuration we were able to maintain much lower pO_2 and which enabled us to keep GDC10 in the MIEC regime and to get high rate of ambipolar diffusion of oxygen, which was necessary for getting high hydrogen production flux by water-splitting in non-galvanic mode. In general, the mixed ionic-electronic conduction in LNO in reducing conditions is relatively much higher than that in doped ceria [18], which indicates that the ambipolar diffusion of oxygen in the LNO/GDC10 bilayer and the resultant hydrogen production are mainly controlled by the GDC10 layer. Therefore, the process of MWHP using LNO/GDC10 can be controlled by varying the total thickness of the LNO/GDC10 bilayer and the relative thickness of the GDC10 layer. As it is already mentioned in the Section 1, in a bilayer structure the gradient within each layer is determined by the relative thickness and transport property of the individual layers [11]; however, any manipulation of the relative thickness of the individual layers in a LNO/GDC10 bilayer of fixed thickness should be done in such a manner that pO_2 at the interface is high enough to prevent LNO degradation, but at the same time it should be low enough to maintain GDC10 in the MIEC regime. The performance of ceria-based bilayers in MWHP may be further improved by changing the dopants and their concentrations to improve the mixed ion-electron conductivity in gadolinium-doped ceria in a reducing atmosphere.

4. Conclusion

The properties of the LNO/GDC10 bilayer were investigated in MWHP as a function of temperature, CO content in the reducing gas and the pO_2. The hydrogen production process was thermally activated and the hydrogen production flux increased with increasing oxygen chemical potential and pH_2O, to yield a maximum of 0.12 cm^3 (STP)/min-cm^2 with 23.25% CO/76.75% CO_2 (40 sccm)/balance He (60 sccm) gas mixture on the oxygen-permeate side and wet N_2 ($pH_2O = 0.49$ atm) on the oxidizing side at 900 °C. The presence of the GDC10 layer on the low pO_2 side protected the LNO layer from coming into the direct contact with very low pO_2, which enabled a high pO_2 gradient to be maintained across the bilayer, thereby generating a stable and high hydrogen production flux in MWHP.

Acknowledgment

This study was supported by the Basic Science Research Program through the National Research Foundation of Korea (NRF) funded by the Ministry of Education, Science and Technology (2009-0090172).

References

[1] C.Y. Park, T.H. Lee, S.E. Dorris, Y. Lu, U. Balachandran, Oxygen permeation and coal-gas-assisted hydrogen production using oxygen transport membranes, Journal of Hydrogen Energy 36 (2011) 9345–9354.
[2] R.W. Baker, Future directions of membrane gas separation technology, Industrial & Engineering Chemistry Research 41 (2002) 1393–1411.
[3] S.J. Song, J.H. Moon, T.H. Lee, S.E. Dorris, U. Balachandran, Thickness dependence of hydrogen permeability for Ni-$BaCe_{0.8}Y_{0.2}O_{3-\delta}$, Solid State Ionics 179 (2008) 1854–1857.
[4] S. Yun, H. Lim, S.T. Oyama, Experimental and kinetic studies of the ethanol steam reforming reaction equipped with ultrathin Pd and Pd–Cu membranes for improved conversion and hydrogen yield, Journal of Membrane Science 409 (2012) 222–231.
[5] S.Y. Jeon, M.B. Choi, C.N. Park, E.D. Wachsman, S.J. Song, High sulfur tolerance dual-functional cermet hydrogen separation membranes, Journal of Membrane Science 382 (2011) 323–327.
[6] U. Balachandran, T.H. Lee, S. Wang, S.E. Dorris, Use of mixed conducting membranes to produce hydrogen by water dissociation, International Journal of Hydrogen Energy 29 (2004) 291–296.
[7] U. Balachandran, T.H. Lee, S.E. Dorris, Hydrogen production by water dissociation using mixed conducting dense ceramic membranes, International Journal of Hydrogen Energy 32 (2007) 451–456.
[8] V.V. Kharton, A.A. Yaremchenko, A.V. Kovalevsky, A.P. Viskup, E.N. Naumovich, P.F. Kerko, Perovskite-type oxides for high-temperature oxygen separation membranes, Journal of Membrane Science 163 (1999) 307–317.
[9] S. Ihara, Approximations for the thermodynamic properties of high-temperature dissociated water vapour, Bulletin of the Electrotechnical Laboratory 41 (1977) 259–280.
[10] R.V. Franca, A. Thursfield, I.S. Metcalfe, $La_{0.6}Sr_{0.4}Co_{0.2}Fe_{0.8}O_{3-\delta}$ microtubular membranes for hydrogen production from water splitting, Journal of Membrane Science 389 (2012) 173–181.
[11] E.D. Wachsman, T.L. Clites, Stable mixed-conducting bilayer membranes for direct conversion of methane to syngas, Journal of the Electrochemical Society 149 (2002) A242–A246.
[12] U. Balachandran, S.E. Dorris, J.E. Emerson, T.H. Lee, Y. Lu, C.Y. Park, J.J. Picciolo, Hydrogen production by water dissociation using ceramic membranes, Annual Report for FY 2008, Argonne National Laboratory (2009).
[13] K.E. Colombo, V.V. Kharton, A.P. Viskup, A.V. Kovalevsky, A.L. Shaula, O. Bolland, Simulation of a mixed-conducting membrane-based gas turbine power plant for CO_2 capture: system level analysis of operation stability and individual process unit degradation, Journal of Solid State Electrochemistry 15 (2011) 329–347.
[14] S.Y. Jeon, M.B. Choi, H.N. Im, J.H. Hwang, S.J. Song, Oxygen ionic conductivity of $La_2NiO_{4+\delta}$ via interstitial oxygen defect, Journal of Physics and Chemistry of Solids 73 (2012) 656–660.
[15] J.R. Frade, V.V. Kharton, A.A. Yaremchenko, E.V. Tsipis, A.L. Shaula, E.N. Naumovich, A.V. Kovalevsky, F.M. Marques, Mixed conducting materials for partial oxidation of hydrocarbons, Boletin de la Sociedad Espanola de Ceramica y Vidrio 43 (2004) 640–643.

[16] M.A. Dragan, Defect chemistry, transport properties and thermodynamic stability of acceptor doped and undoped layered La_2NiO_4, PhD Thesis, RWTH Aachen University (2006).
[17] A.J. Jacobson, Materials for solid oxide fuel cells, Chemistry of Materials 22 (2010) 660–674.
[18] R.N. Blumenthal, F.S. Brugner, J.E. Garnier, The electrical conductivity of CaO-doped nonstoichiometric cerium dioxide from 700° to 1500 °C, Journal of the Electrochemical Society 120 (1973) 1230–1237.
[19] M.B. Choi, K.T. Lee, H.S. Yoon, S.Y. Jeon, E.D. Wachsman, S.J. Song, Electrochemical properties of ceria based IT-SOFC using the $La_{0.1}Sr_{0.9}Co_{0.8}Fe_{0.2}O_{3-\delta}$ as a cathode, Journal of Power Sources 220 (2012) 377–382.
[20] K.T. Lee, D.W. Jung, M.A. Camaratta, H.S. Yoon, J.S. Ahn, E.D. Wachsman, $Gd_{0.1}Ce_{0.9}O_{1.95}/Er_{0.4}Bi_{1.6}O_3$ bilayered electrolytes fabricated by a simple colloidal route using nano-sized $Er_{0.4}Bi_{1.6}O_3$ powders for high performance low temperature solid oxide fuel cells, Journal of Power Sources 205 (2012) 122–128.
[21] M.B. Choi, S.Y. Jeon, J.S. Lee, H.J. Hwang, S.J. Song, Chemical diffusivity and ionic conductivity of $GdBaCo_2O_{5+\delta}$, Journal of Power Sources 195 (2010) 1059–1064.
[22] M.B. Choi, S.Y. Jeon, H.J. Hwang, J.Y. Park, S.J. Song, Composite of $Ce_{0.8}Gd_{0.2}O_{2-\delta}$ and $GdBaCo_2O_{5+\delta}$ as oxygen separation membranes, Solid State Ionics 181 (2010) 1680–1684.
[23] S.J. Song, J.H. Moon, H.W. Ryu, T.H. Lee, S.E. Dorris, U. Balachandran, Non-galvanic hydrogen production by water splitting using cermet membranes, Journal of Ceramic Processing Research 9 (2008) 123–125.
[24] G.W. Castellan, in: Physical Chemistry, 3rd ed., University of Maryland, Collage Park, MD, 1957 p 85.
[25] H.S. Kim, H.I. Yoo, Defect-chemical analysis of the nonstoichiometry, conductivity and thermopower of $La_2NiO_{4+\delta}$, Physical Chemistry Chemical Physics 12 (2010) 4704–4713.
[26] T.H. Lee, Y.L. Yang, A.J. Jacobson, Oxygen permeation in dense $SrCo_{0.8}Fe_{0.2}O_{3-\delta}$ membranes: surface exchange kinetics versus bulk diffusion, Solid State Ionics 100 (1997) 77–85.
[27] H.J.M. Bouwmeester, A.J. Burggraaf, Dense ceramic membranes for oxygen separation, in: P.J. Gellings, H.J.M. Bouwmeester (Eds.), The CRC Handbook of Solid State Electrochemistry, CRC Press, Boca Raton, FL, 1997.
[28] S.Y. Jeon, M.B. Choi, J.H. Hwang, E.D. Wachsman, S.J. Song, Oxygen excess nonstoichiometry and thermodynamic quantities of $La_2NiO_{4+\delta}$, Journal of the Electrochemical Society 16 (2012) 785–793.
[29] T.H. Kwon, T.W. Lee, H.I. Yoo, Partial electronic conductivity and electrolytic domain of bilayer electrolyte $Zr_{0.84}Y_{0.16}O_{1.92}/Ce_{0.9}Gd_{0.1}O_{1.95}$, Solid State Ionics 195 (2011) 25–35.
[30] C.Y. Park, F.V. Azzarello, A.J. Jacobson, The oxygen nonstoichiometry and electrical conductivity of $La_{0.7}Sr_{0.3}Cu_{0.2}Fe_{0.8}O_{3-\delta}$, Journal of Materials Chemistry 16 (2006) 3624–3628.
[31] H.N. Im, S.Y. Jeon, M.B. Choi, J.Y. Park, S.J. Song, Chemical expansion of water splitting oxygen separation membranes of $La_{0.7}Sr_{0.3}Cu_{0.2}Fe_{0.8}O_{3-\delta}$, Journal of Ceramic Processing Research 13 (5) (2012) 579–585.
[32] S.H. Park, Tailoring of electrolytic domain of ceria-based electrolytes with electron traps, Ph.D. Thesis (in Korean), Seoul National University, Seoul (2008).
[33] S.H. Park, H.I. Yoo, Defect-chemical role of Mn in Gd-doped CeO_2, Solid State Ionics 176 (2005) 1485–1490.